General Disclaimer

One or more of the Following Statements may affect this Document

- This document has been reproduced from the best copy furnished by the organizational source. It is being released in the interest of making available as much information as possible.

- This document may contain data, which exceeds the sheet parameters. It was furnished in this condition by the organizational source and is the best copy available.

- This document may contain tone-on-tone or color graphs, charts and/or pictures, which have been reproduced in black and white.

- This document is paginated as submitted by the original source.

- Portions of this document are not fully legible due to the historical nature of some of the material. However, it is the best reproduction available from the original submission.

Produced by the NASA Center for Aerospace Information (CASI)

AD-A012 876

HEAT-TRANSFER TESTS ON THE ROCKWELL INTERNATIONAL SPACE SHUTTLE ORBITER WITH AND WITHOUT SIMULATED PROTUBERANCES

L. D. Carter, et al

Arnold Engineering Development Center
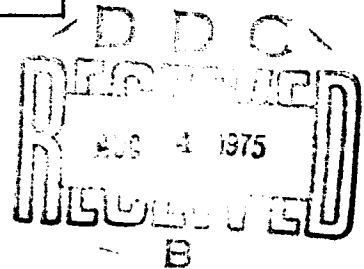
AEDC-TR-75-20

219085

HEAT-TRANSFER TESTS ON THE
ROCKWELL INTERNATIONAL SPACE SHUTTLE ORBITER
WITH AND WITHOUT SIMULATED PROTUBERANCES

AD AU12876

VON KÁRMÁN GAS DYNAMICS FACILITY
ARNOLD ENGINEERING DEVELOPMENT CENTER
AIR FORCE SYSTEMS COMMAND
ARNOLD AIR FORCE STATION, TENNESSEE 37389

July 1975

Final Report for Period March 1 — July 31, 1974

D D C

AUG 4 1975

B

Prepared for

NATIONAL AERONAUTICS AND SPACE ADMINISTRATION (JSC)
HOUSTON, TEXAS 77958

NOTICES

When U. S. Government drawings specifications, or other data are used for any purpose other than a definitely related Government procurement operation, the Government thereby incurs no responsibility nor any obligation whatsoever, and the fact that the Government may have formulated, furnished, or in any way supplied the said drawings, specifications, or other data, is not to be regarded by implication or otherwise, or in any manner licensing the holder or any other person or corporation, or conveying any rights or permission to manufacture, use, or sell any patented invention that may in any way be related thereto.

Qualified users may obtain copies of this report from the Defense Documentation Center.

References to named commercial products in this report are not to be considered in any sense as an endorsement of the product by the United States Air Force or the Government.

This report has been reviewed by the Information Office (OI) and is releasable to the National Technical Information Service (NTIS). At NTIS, it will be available to the general public, including foreign nations.

APPROVAL STATEMENT

This technical report has been reviewed and is approved for publication.

FOR THE COMMANDER

JIMMY W. MULLINS
Lt Colonel, USAF
Chief Air Force Test Director, VKF
Directorate of Test

FRANK J. PASSARELLO
Colonel, USAF
Director of Test

REPORT DOCUMENTATION PAGE		READ INSTRUCTIONS BEFORE COMPLETING FORM
1 REPORT NUMBER AEDC-TR-75-20	2 GOVT ACCESSION NO.	3. RECIPIENT'S CATALOG NUMBER
4 TITLE (and Subtitle) HEAT-TRANSFER TESTS ON THE ROCKWELL INTERNATIONAL SPACE SHUTTLE ORBITER WITH AND WITHOUT SIMULATED PROTUBERANCES		5. TYPE OF REPORT & PERIOD COVERED Final Report, March 1 - July 31, 1974
		6. PERFORMING ORG. REPORT NUMBER
7 AUTHOR(s) L. D. Carter and C. E. Kaul, ARO, Inc.		8. CONTRACT OR GRANT NUMBER(s)
9 PERFORMING ORGANIZATION NAME AND ADDRESS Arnold Engineering Development Center (XO) Arnold Air Force Station, TN 37389		10. PROGRAM ELEMENT, PROJECT, TASK AREA & WORK UNIT NUMBERS Program Element 921E Project 9705
11. CONTROLLING OFFICE NAME AND ADDRESS National Aeronautics and Space Administration (JSC), Houston, Texas 77958		12. REPORT DATE July 1975
		13. NUMBER OF PAGES 38
14 MONITORING AGENCY NAME & ADDRESS(if different from Controlling Office)		15. SECURITY CLASS. (of this report) UNCLASSIFIED
		15a. DECLASSIFICATION DOWNGRADING SCHEDULE N/A

16. DISTRIBUTION STATEMENT (of this Report)

Approved for public release; distribution unlimited.

17. DISTRIBUTION STATEMENT (of the abstract entered in Block 20, if different from Report)

18. SUPPLEMENTARY NOTES

Available in DDC.

19. KEY WORDS (Continue on reverse side if necessary and identify by block number)

aerodynamic heating

heat transfer

reentry vehicles

20 ABSTRACT (Continue on reverse side if necessary and identify by block number)
    Aerothermodynamic tests on the forward half of the Rockwell International Space Shuttle Orbiter Configuration 140C were conducted at Mach number 8. The phase-change paint and thin-skin thermocouple techniques were used to determine the aerodynamic heating rates on the Orbiter models during simulated atmospheric reentry. Smooth 0.04-scale models and models with scaled protuberances and indentations which simulated the windshields,

DD FORM 1 JAN 73 1473   EDITION OF 1 NOV 65 IS OBSOLETE

20, Continued

cargo bay door hinges, vents, and thruster nozzles were tested
over an angle-of-attack range from 20 to 45 deg at yaw angles
from -5 to 5 deg and at Reynolds numbers, based on the total
Orbiter scaled length, from 2.15 to 15.9 million. Comparisons
of the model heat-transfer rates obtained with a smooth surface
and with scaled protuberances are presented.

AFSC
Arnold AFS Tenn

PREFACE

CONTENTS

ILLUSTRATIONS

Figure

TABLES

1.0 INTRODUCTION

These studies were undertaken to define the effects of simulated protuberances such as door hinges, thruster nozzles, windows, etc., on local heating rates and boundary-layer transition for the 140C Space Shuttle Orbiter configuration. To provide an adequate definition of heating rate distributions in the protuberance regions it was necessary to scale the models as large as possible. A 4-percent model scale was obtained by simulating only the forward half of the Orbiter (L/2 = 25.8 in.).

The tests were conducted in two parts: the first involved the phase-change paint technique, and the second utilized the thin-skin thermocouple technique to obtain heating rates. The data were obtained in the Hypersonic Wind Tunnel (B) of the von Kármán Gas Dynamics Facility (VKF) at a nominal Mach number of 8. Angle of attack was varied from 20 to 45 deg at free-stream Reynolds numbers from 2.15 to 15.9 million based on the scaled Orbiter's full length (L = 51.6 in.).

2.0 APPARATUS

2.1 WIND TUNNEL

Tunnel B is a continuous, closed-circuit, variable density wind tunnel equipped with $M_\infty = 6$ and 8 axisymmetric contoured nozzles and a 50-in.-diam test section. The tunnel can be operated at nominal Mach numbers of 6 or 8 at stagnation pressures from 20 to 300 and 50 to 900 psia, respectively, and at stagnation temperatures up to $1350°R$. The model can be injected into the tunnel for a test run and then retracted for model cooling and model changes without stopping the tunnel flow. A more complete description of the tunnel is presented in Ref. 1.

2.2 MODELS

The models were 0.04-scale models of the forward half of the Rockwell International Space Shuttle Orbiter 140C. All models were supplied by Rockwell. The contours of these models are defined by Rockwell drawing VL70-000 140C. The two configurations tested were a smooth surface model and a model with protuberances and indentations which simulated the windshields, cargo bay door hinges, vents, and thruster nozzles.

2.2.1 Phase-Change Paint Models

A sketch of a phase-change paint model is shown in Fig. 1, and a photograph of a protuberance model is shown in Fig. 2. To facilitate testing, three duplicate smooth models and two duplicate protuberance models were used during the tests. These models

were designated as Model 82-0 by Rockwell. Lockheed Missiles and Space Company (LMSC) of Huntsville, Alabama, subcontractors for model fabrication, cast the models from a proprietary epoxy material (Material LH), which has a low thermal diffusivity and relatively high strength. The models were cast as a one-piece shell with a nominal wall thickness of 1 in. and then filled with foam. Samples of the same batch of epoxy used to cast the models were analyzed by LMSC to determine the thermophysical properties (density, specific heat, and conductivity) which were necessary for data reduction.

2.2.2 Thermocouple Model

The thin-skin thermocouple model had structural and thin-skin areas constructed of 17-4 PH stainless steel. The skin thickness at the instrumentation areas was nominally 0.030 in. There were no movable or removable parts on the model, and it was designated as Model 83-0. Only one thin-skin model was supplied by Rockwell, and it was constructed so that the pilot-right side had a smooth surface and the pilot-left side had the simulated protuberances.

A sketch of the model is shown in Fig. 3. The orientation of the pilot-left protuberances is as shown in the figure. The smooth side (pilot-right) thermocouple locations and the maximum-half-breath line (MHB) are indicated in Fig. 3b. The protuberances on the thin-skin model are the same as those simulated on the phase-change paint models, with the exception of the forward firing thrusters, nose wheel-well doors, and the pilot-right-side fuselage vent. The forward firing thrusters were deleted from the paint protuberance models, whereas the thermocouple model lacked the wheel-well doors and pilot-right fuselage vent. The model was instrumented with 477 iron-constantan thermocouples as illustrated in Fig. 3.

2.3 INSTRUMENTATION

The tunnel stilling chamber pressure was measured with a 1000-psid transducer referenced to near vacuum and having full-scale calibrated ranges of 100 and 1000 psi. The precision of this transducer is estimated to be ±0.2 percent of the calibrated range. Stilling chamber temperature was measured with a Chromel®Alumel® thermocouple which has a precision of ±0.5 percent based on the thermocouple wire manufacturer's specification.

3.0 PROCEDURES

3.1 TEST CONDITIONS

The nominal test conditions for the two test phases are listed below. Complete test summaries for both the phase-change paint and the thin-skin thermocouple test entries are given in Tables 1 and 2, respectively.

6

M_∞	p_o,psia	T_o,°R	h_{ref}, Btu/ft²-sec-°R	$Re_\infty \times 10^{-6}$, ft⁻¹	Data Type
7.90	110	1,270	0.0116	0.5	P,TC
7.94	210	1,270	0.0162	1.0	P,TC
7.97	325	1,280	0.0199	1.5	P
7.98	430	1,300	0.0230	2.0	P,TC
7.99	675	1,340	0.0289	3.0	TC
8.00	860	1,350	0.0325	3.7	TC

Note: P = phase-change paint;
TC = thin-skin thermocouple.

Uncertainties of the basic tunnel flow parameters p_o, T_o, and M_∞ were estimated from repeat calibrations of the instruments and from repeatability and uniformity of the test section flow during tunnel calibrations. The individual contributions of these uncertainties were used to compute the uncertainties in the other parameters dependent on these by means of the Taylor series method of error propagation.

Parameter	Uncertainty, Percent
p_o	±0.5
T_o	±0.5
M_∞	±0.3
h_{ref}	±0.8
Re_∞	±1.2

3.2 TEST PROCEDURES, DATA REDUCTION, AND DATA PRECISION

3.2.1 Phase-Change Paint

For phase-change paint tests, the data were reduced by assuming that the model wall heating can be represented by a thermally semi-infinite slab (Refs. 2 and 3). A material with a low thermal diffusivity is necessary for this assumption to be valid for reasonable model wall thicknesses and testing times.

The phase-change paint technique of obtaining heat-transfer data uses a fusible coating which changes from an opaque solid to a transparent liquid (i.e., it melts) at a specified temperature (T_{pc}). The demarcations between melted and unmelted paint (melt lines) are model surface isotherms and are used to compute the aerodynamic heating. Tempilaq® paint was used as the phase-change coating for these tests. The calibrated melting points of the paints used were 113, 125, 131, 150, 169, 175, 194, 200, 225, 250, 275, 300, 350, and 400°F. A more complete description of the phase-change paint technique is presented in Ref. 3.

After the model was painted with the appropriate Tempilaq paint, it was installed on the tunnel sting, and the model surface initial temperature (T_{wi}) was measured with a thermocouple probe. The model was positioned to the test attitude and injected into the tunnel flow for about 40 sec. During this time four 70-mm sequence cameras using black and white film photographed the progression of the paint melt lines. These cameras were triggered simultaneously at a nominal rate of one frame/sec while an analog-to-digital scanner recorded the precise timing on magnetic tape. After the model was retracted from the tunnel flow, it was removed from the sting and cooled and cleaned with an alcohol bath before being repainted for the next test run.

Data reduction of the melt line photographs was accomplished by making tracings of these isothermal lines for various times during the test run. The lines of each of these tracings were related to corresponding aerodynamic heat-transfer coefficients, h, by applying the semi-infinite slab heat equation, given below.

$$\left(\frac{T_{pc} - T_i}{T_{aw} - T_i}\right) = 1 - e^{\beta^2} \text{ erfc } \mu$$

where

$$\beta = \frac{h\sqrt{\Delta t}}{\sqrt{wc_p k}}$$

and

$$\Delta t = \text{time of heating}$$

The lumped material thermophysical property $\sqrt{wc_p k}$ was a function of temperature (See Table 3). The heat-transfer coefficients were computed for an assumed adiabatic recovery temperature (T_{aw}) of T_o. The Fay-Riddell stagnation point heat-transfer coefficient (Ref. 4), h_{ref}, based on a 0.04-ft-radius sphere, was used to normalize the computed aerodynamic heat-transfer coefficients. (The radius of this hypothetical sphere would be 1 ft at corresponding Orbiter full-scale conditions.)

An accurate estimate of the precision of phase-change paint data is hampered by the fact that an observer must determine the location of the melt line (Ref. 5). For the results presented in this report only uncertainties attributable to the measured parameters are considered. The parameters needed for the solution of the equation for the heat-transfer coefficient, h, are T_o, T_{pc}, T_i, $\sqrt{wc_p k}$, and Δt. The nominal uncertainties in these specific parameters are summarized below.

Parameter	Uncertainty, Percent
Δt	± 1.0
$\sqrt{wc_p k}$	± 10.0
T_i	± 0.5
T_o	± 0.5
T_{pc}	± 0.5

Combining the above measurement uncertainties using the Taylor Series method of error propagation yields

for $T_{pc} \leqslant 200°F$, h uncertainty $\approx \pm 13$ percent

for $T_{pc} > 200°F$, h uncertainty $\approx \pm 11$ percent

3.2.2 Thermocouple Data

Thermocouple outputs were recorded using the VKF digital data scanner in conjunction with a Beckman 210 digital data system. The thermocouple readings were scanned at the rate of 20 times/sec from the start of the model injection cycle until about 3 sec after the model reached tunnel centerline. After each retraction the model was cooled to an isothermal state using high-pressure air.

The reduction of thin-skin thermocouple data normally involves only the calorimetric heat balance which, in coefficient form, is

$$h = wbc_p \frac{dT_w/dt}{T_o - T_w} \tag{1}$$

Radiation and conduction losses are neglected in this heat balance, and data reduction simply requires evaluation of dT_w/dt from the temperature-time data and determination of model properties. For the present tests radiation effects were negligible; however, conduction effects were significant in several regions of the model. To permit identification of these regions and improve evaluation of the data, the following procedure was used.

Separation of variables and integration of Eq. (1), assuming constant w, b, c_p, and T_o, yields

$$\frac{h}{wbc_p} (t - t_i) = \ln\left[\frac{T_o - T_{wi}}{T_o - T_w}\right] \tag{2}$$

9

Differentiation of Eq. 2 with respect to time gives

$$\frac{h}{wbc_p} = \frac{d}{dt} \; \ell n \left[\frac{T_o - T_{wi}}{T_o - T_w} \right]$$

Since h/wbc_p is a constant, plotting $\ell n(T_o - T_{wi})/(T_o - T_w)$ versus time gives a straight line if conduction is negligible. Thus, deviations from a straight line can be interpreted as conduction effects.

The data were evaluated in this manner and generally a reasonably linear portion of the curve could be found for all thermocouples. A linear least-squares curve fit of

$$\ell n \left(\frac{T_o - T_{wi}}{T_o - T_w} \right)$$

versus time was applied to the data beginning at the time when the model reached uniform flow and extending for a time span which was a function of the heating rate, as shown below.

Heating Rate, °R/sec	Number of Data Points	Time Span, sec
$dT_w/dt > 32$	5	0.20
$16 < dT_w/dt \leqslant 32$	7	0.30
$8 < dT_w/dt \leqslant 16$	9	0.40
$4 < dT_w/dt \leqslant 8$	13	0.60
$2 < dT_w/dt \leqslant 4$	17	0.80
$1 < dT_w/dt \leqslant 2$	25	1.20
$dT_w/dt \leqslant 1$	41	2.00

The time spans given above were nominally adequate to keep the evaluation of the right side of Eq. (2) within the linear region.

In practice, the value of c_p is not constant as assumed and the relation

$$c_p = 0.0797 + (5.556 \times 10^{-5})T_w$$

was used with the value of T_w at the midpoint of the curve fit. The maximum variation of c_p over any curve fit was less than 1.2 percent; thus, the assumption of constancy was not grossly violated. A constant value of 490.0 lbm/ft³ was used for w (17-4 PH stainless steel) with the measured values of b for each thermocouple. Uncertainties in the values of heat-transfer coefficient based on the Taylor series method of error propagation are tabulated as follows:

10

h	Uncertainty, Percent
10^{-2}	5
10^{-3}	7
10^{-4}	10

A general summary of the thin-skin thermocouple technique may be found in Ref. 6.

4.0 RESULTS AND DISCUSSION

Since the aerodynamic heating generated by turbulent boundary-layer flow may be several times greater than that for laminar flow at the same flight attitude and conditions, it is important to examine not only the general levels of heating but also the factors affecting flow transition from laminar to turbulent. The tests reported herein were designed to determine the effects that various protuberances had on both the local heat rates and those over the entire model caused by early or premature flow transition.

The model windward centerline data are presented in Figs. 4, 5, and 6. As expected, the laminar nose heating rate distributions for various free-stream Reynolds numbers are well correlated by the Fay-Riddell reference level (h_{ref}). For the two lower Reynolds numbers, laminar flow persisted along the entire length of the body for the angle-of-attack range from 20 to 45 degrees. At a = 20 deg (Fig. 4) the beginning of transition appeared near the aft end of the model ($X/L \approx 0.4$) for the higher Reynolds numbers. This is shown by the divergence from the laminar level of the lower Reynolds number heating in this region. As the angle of attack was increased to 30 deg (Fig. 5), the location of beginning of transition moved forward until at a = 40 deg, Fig. 6, it had reached the center of the body ($X/L \approx 0.25$). At this test condition ($Re_{\infty,L}$ = 15.9 x 10^6), the heating rates along the aft end of the model were about 70 percent of the rates on the nose.

The shaded symbols in Fig. 5 indicate the heat-rate levels as determined with Tempilaq paint. The agreement between these data and the thin-skin data is considered quite good.

One of the objectives of this test was to evaluate the effects of the grooves, which simulated the nose wheel-well doors, on the windward surface heat rates. A comparison of the windward centerline heat-rate data from both the smooth and protuberance paint models and from the thin-skin model is presented in Fig. 7. The thin-skin and smooth paint model data are in good agreement and indicate a laminar distribution along the full length of the smooth surface model. The heat-rate distribution for the protuberance model followed the laminar distribution to an X/L value of about 0.2, where it diverged.

This increase in the protuberance model heat rates indicates that the wheel-well door grooves probably acted as boundary-layer trips, causing premature transition.

Two major areas of interest regarding data generated from these tests were the measurement of overall leeward heat-transfer-rate distributions and identification of any localized protuberance-related heating. Leeward centerline heat-transfer-rate distributions for the paint and thermocouple model at $Re_{\infty,L}$ = 8.6 million are presented in Fig. 8. Comparison of Fig. 8 with Figs. 5 and 6 demonstrates that peak heating rates in the canopy region (0.15 ⩽ X/L ⩽ 0.20) are of the same magnitude as the lower values measured on the windward centerline. No protuberance-related heating rate variations are noted in this region.

A substantial Reynolds number effect on the measured heating rates in the canopy region (X/L = 0.15) at 20 deg angle of attack is shown in Fig. 9. In Fig. 10 oil-flow photographs at $Re_{\infty,L}$ = 4.3 million are presented. Fig. 10a, at 20 deg angle of attack, clearly defines a region of separated flow along the top centerline starting near X/L = 0.08 and ending on the canopy at X/L = 0.15. This is consistent with the data for the two lower Reynolds numbers in Fig. 9. The heating rates at the higher Reynolds numbers for 20 deg angle of attack in the nose-canopy region are indicative of attached flow which impinges directly on the canopy.

Pilot-right-side maximum-half-breadth (MHB) line heat-transfer-rate distributions for the thermocouple model at $Re_{\infty,L}$ = 4.3 million are presented in Fig. 11. The negative 5-deg yaw peak heat-transfer rate at 20 deg angle of attack and X/L ≈ 0.3 approaches windward centerline rates at the same model station (see Fig. 4). This peak is produced by the wing-glove leading-edge trailing vortex impingement on the fuselage (Fig. 12a). As is evident in these oil-flow photographs, the orientation of this vortex streak on the model surface shifts with changes in angle of attack. Additional evidence of the vortex-induced heating is shown in the sequence of phase-change paint photographs presented in Fig. 13. Comparison of the left and right sides of the figure shows that in this case the protuberances had observable effects on local heating rates but produced little effect on the overall heating patterns.

5.0 SUMMARY OF RESULTS

Phase-change paint and thin-skin thermocouple heat-transfer tests were conducted to define the heating rates on the forward half of the Rockwell International 140C Configuration Space Shuttle Orbiter at simulated reentry conditions. The Reynolds number, based on the total model scaled length, was varied from 2.15 to 15.9 million over the angle-of-attack range from 20 to 45 deg at a Mach number of 8. Within the limits of the test scope, the following conclusions were reached:

1. A comparison of the windward centerline data for the smooth and protuberance models indicated that the wheel-well door grooves probably promoted boundary-layer transition and thus produced local increases in the heat-transfer rates.

2. Leeward centerline data exhibited Reynolds number/flow separation effects in the nose-canopy region at 20 deg angle of attack.

3. Peak canopy heating rates approach windward centerline values at $X/L \approx$ 0.2.

4. The wing-glove leading edge produced a vortex which at 5 deg negative yaw and 20 deg angle of attack generated heat-transfer rates on the side of the fuselage that approached those of the windward centerline at $X/L \leqslant 0.3$.

5. Simulated protuberances on the leeward surfaces produced measurable local heating effects but no significant changes in the overall heating patterns.

REFERENCES

1. Sivells, James C. "Aerodynamic Design and Calibration of the VKF 50-Inch Hypersonic Wind Tunnels." AEDC-TDR-62-230 (AD299774), March 1963.

2. Martindale, W. R., Matthews, R. K., and Trimmer, L. L. "Heat-Transfer and Flow-Field Tests of the North American Rockwell/General Dynamics Convair Space Shuttle Configurations." AEDC-TR-72-169 (AD755354), January 1973.

3. Jones, Robert A. and Hunt, James L. "Use of Fusible Temperature Indicators for Obtaining Quantitative Aerodynamic Heat-Transfer Data." NASA-TR-R-230, February 1966.

4. Fay, J. A. and Riddell, F. R. "Theory of Stagnation Point Heat Transfer in Dissociated Air." Journal of the Aerospace Sciences, Vol. 25, No. 2, pp. 73-85, 121, February 1958.

5. Nossaman, G. O. "Feasibility Study for Automatic Reduction of Phase Change Imagery." NASA CR-112001, 1971.

6. Trimmer, L. L., Matthews, R. K., and Buchanan, T. D. "Measurement of Aerodynamic Heat Rates at the von Kármán Facility." ICIASF '73, Institute of Electrical and Electronics Engineers, Inc., New York, 1973, pp. 35-44.

Fuselage Vent,
Pilot Right

Nose Wheel-
Well Doors

6.6

8.6
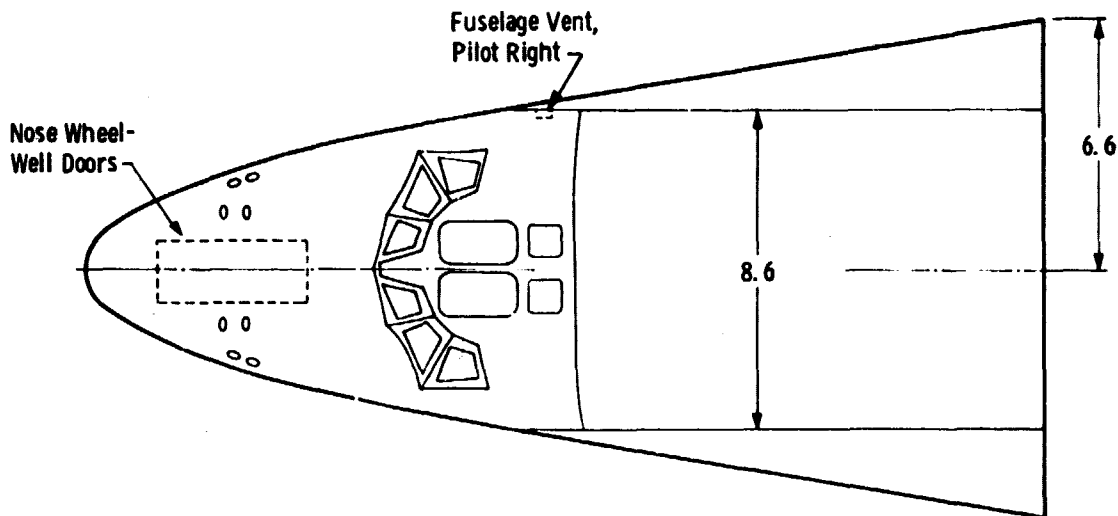
Note: The smooth paint models had the
same basic dimensions as are
shown here but did not have the
protuberances.

All dimensions are in inches.

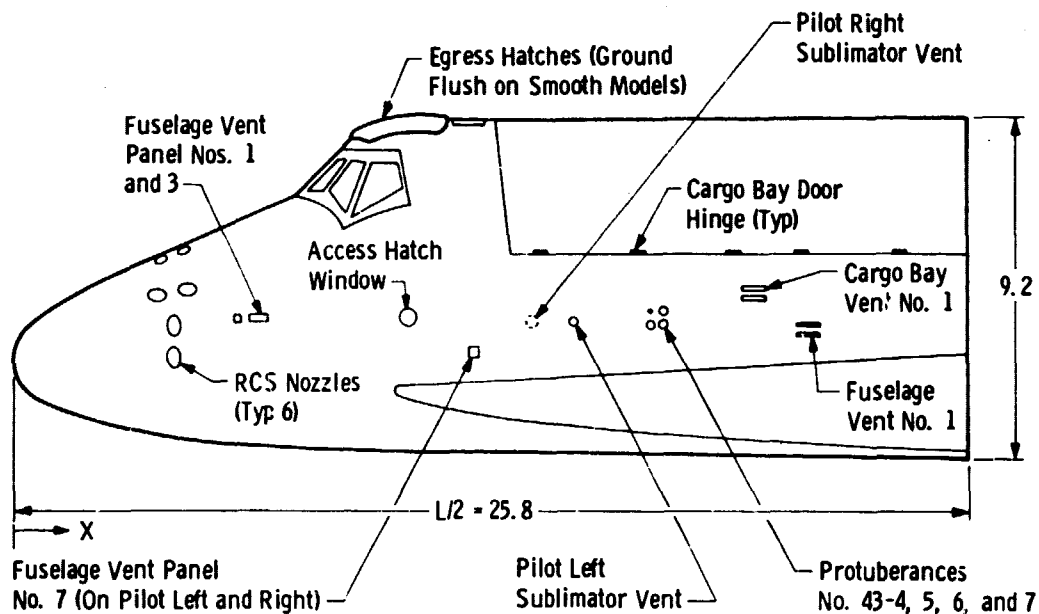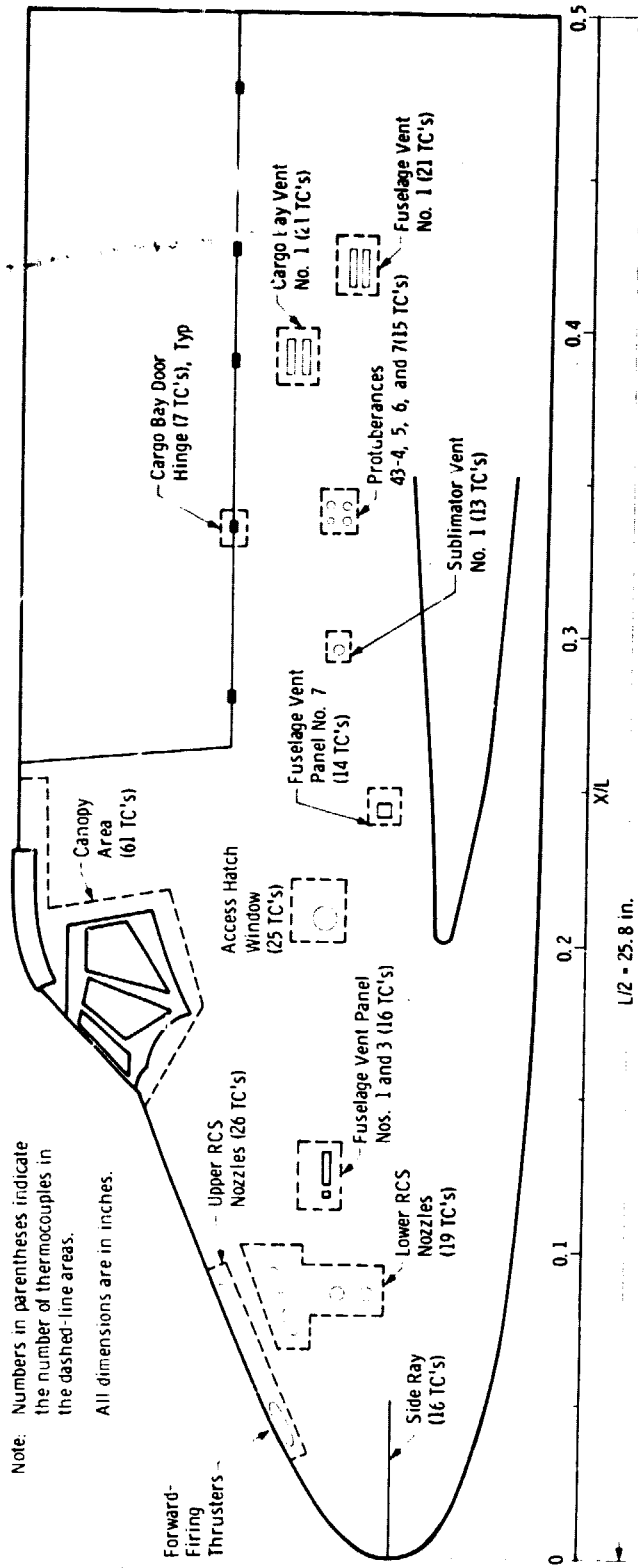Egress Hatches (Ground
Flush on Smooth Models)

Pilot Right
Sublimator Vent

Fuselage Vent
Panel Nos. 1
and 3

Cargo Bay Door
Hinge (Typ)

Access Hatch
Window

Cargo Bay
Vent No. 1

9.2

RCS Nozzles
(Typ 6)

Fuselage
Vent No. 1

L/2 = 25.8

X

Fuselage Vent Panel
No. 7 (On Pilot Left and Right)

Pilot Left
Sublimator Vent

Protuberances
No. 43-4, 5, 6, and 7

Figure 1. Sketch of phase-change paint models.

Preceding page blank

AEDC
74-676

Figure 2. Photograph of the Space Shuttle Orbiter protuberance paint model.

Note. Numbers in parentheses indicate the number of thermocouples in the dashed-line areas.

All dimensions are in inches.

Forward-Firing Thrusters

Upper RCS Nozzles (26 TC's)

Canopy Area (61 TC's)

Access Hatch Window (25 TC's)

Fuselage Vent Panel Nos. 1 and 3 (16 TC's)

Lower RCS Nozzles (19 TC's)

Side Ray (16 TC's)

Cargo Bay Door Hinge (7 TC's), Typ

Fuselage Vent Panel No. 7 (14 TC's)

Cargo Bay Vent No. 1 (21 TC's)

Protuberances 43-4, 5, 6, and 7 (15 TC's)

Fuselage Vent No. 1 (21 TC's)

Sublimator Vent No. 1 (13 TC's)

L/2 = 25.8 in.

X/L

a. Protuberance side (pilot left)

Figure 3. Sketch of the thin-skin thermocouple model.

17
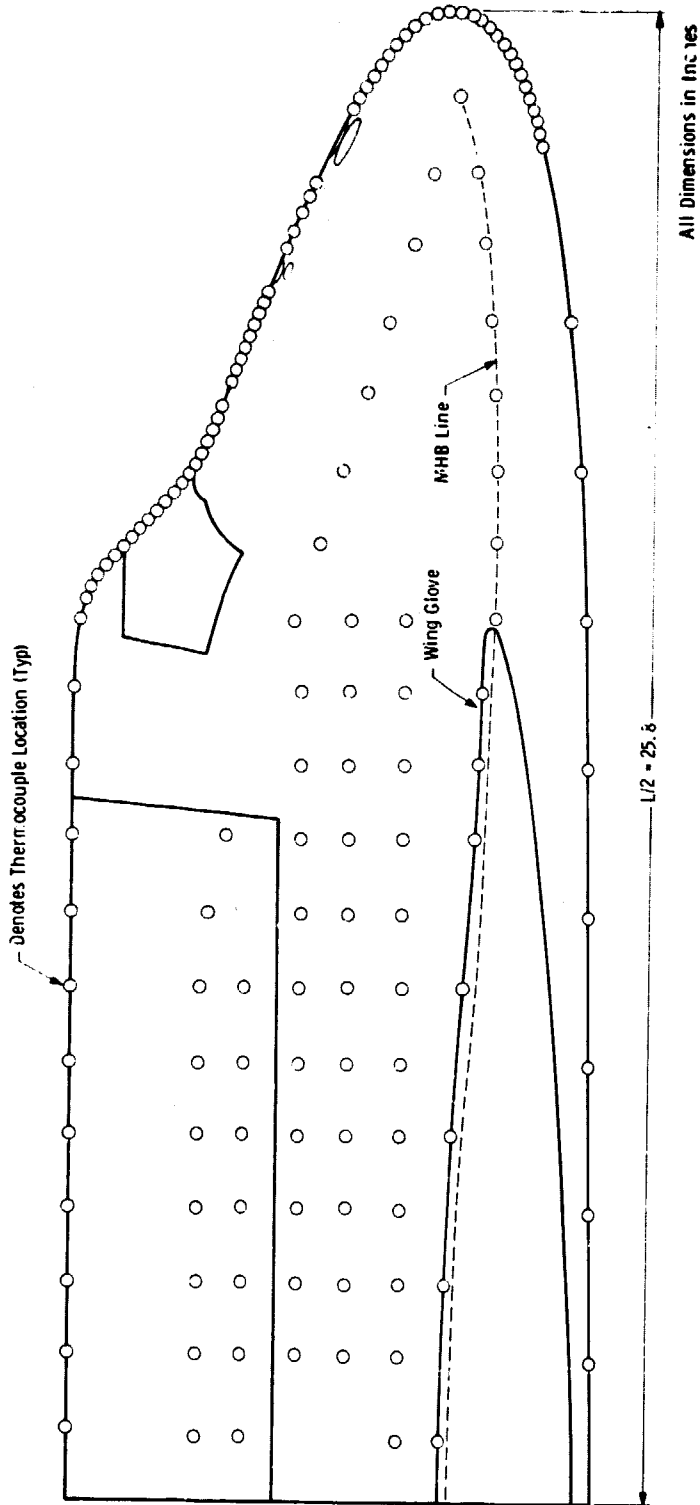
b. Smooth side (pilot right)
Figure 3. Concluded.
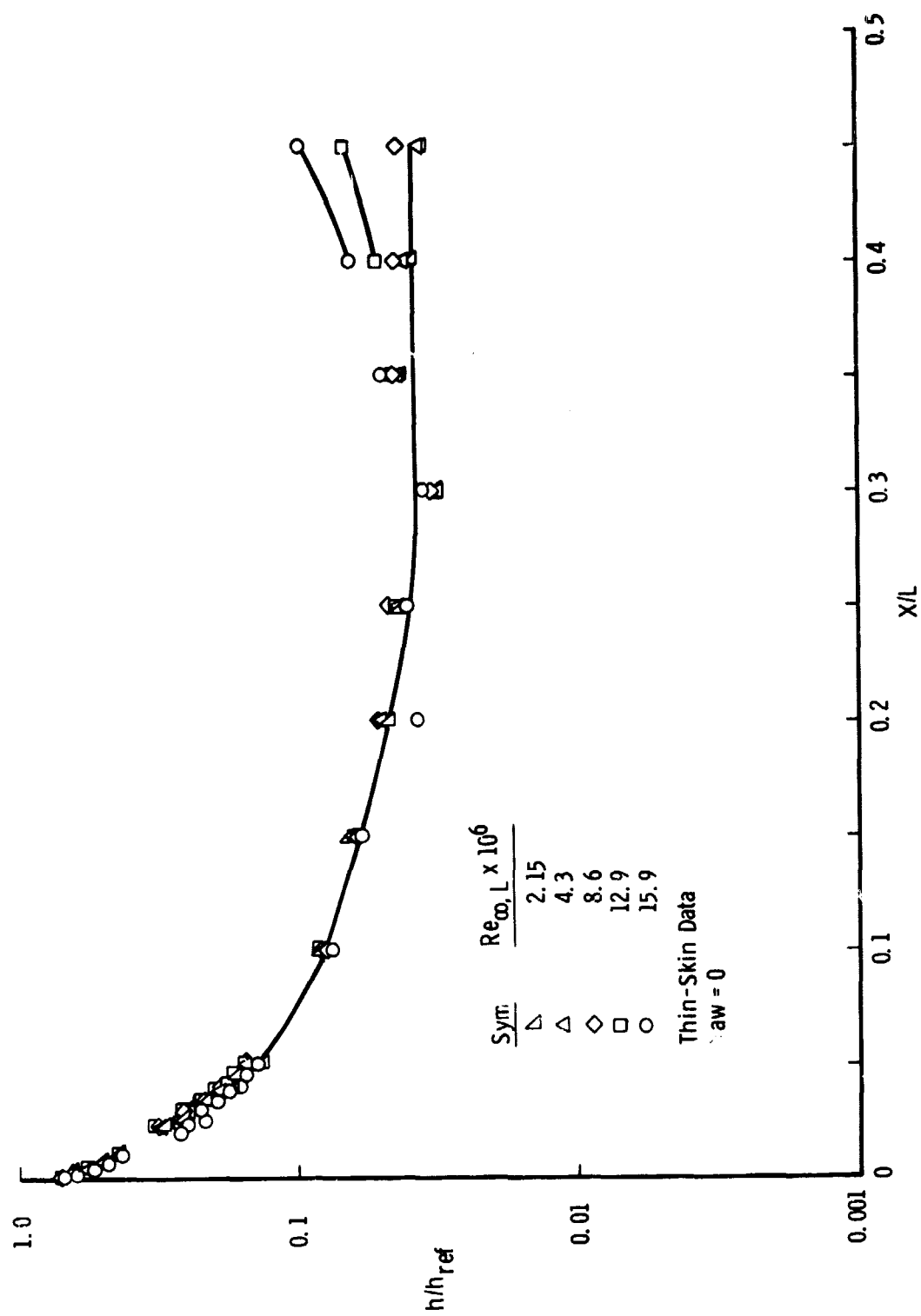
Figure 4. Windward centerline heat-transfer distributions at 20 deg angle of attack.

19
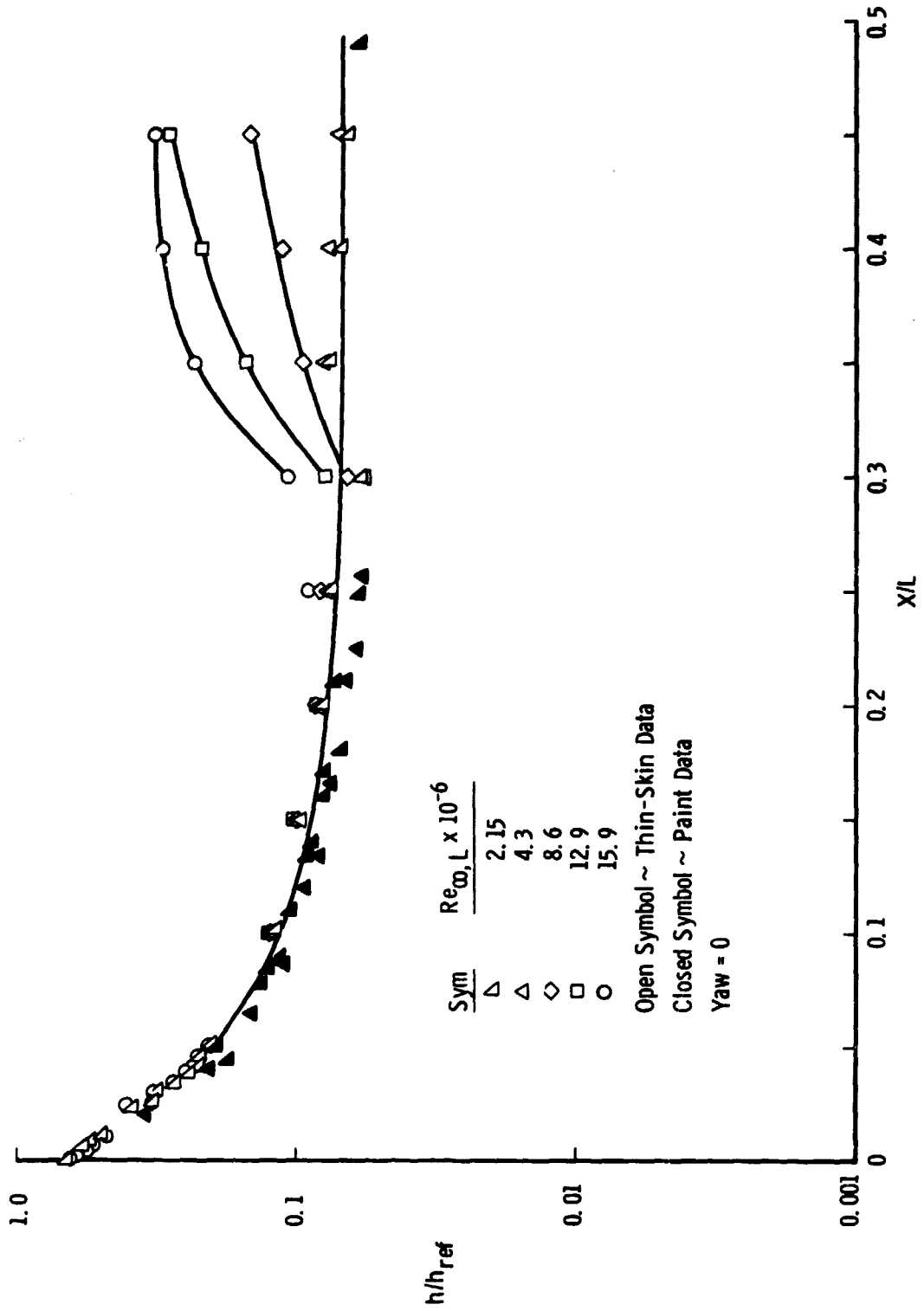
Figure 5. Windward centerline heat-transfer distributions at 30 deg angle of attack.
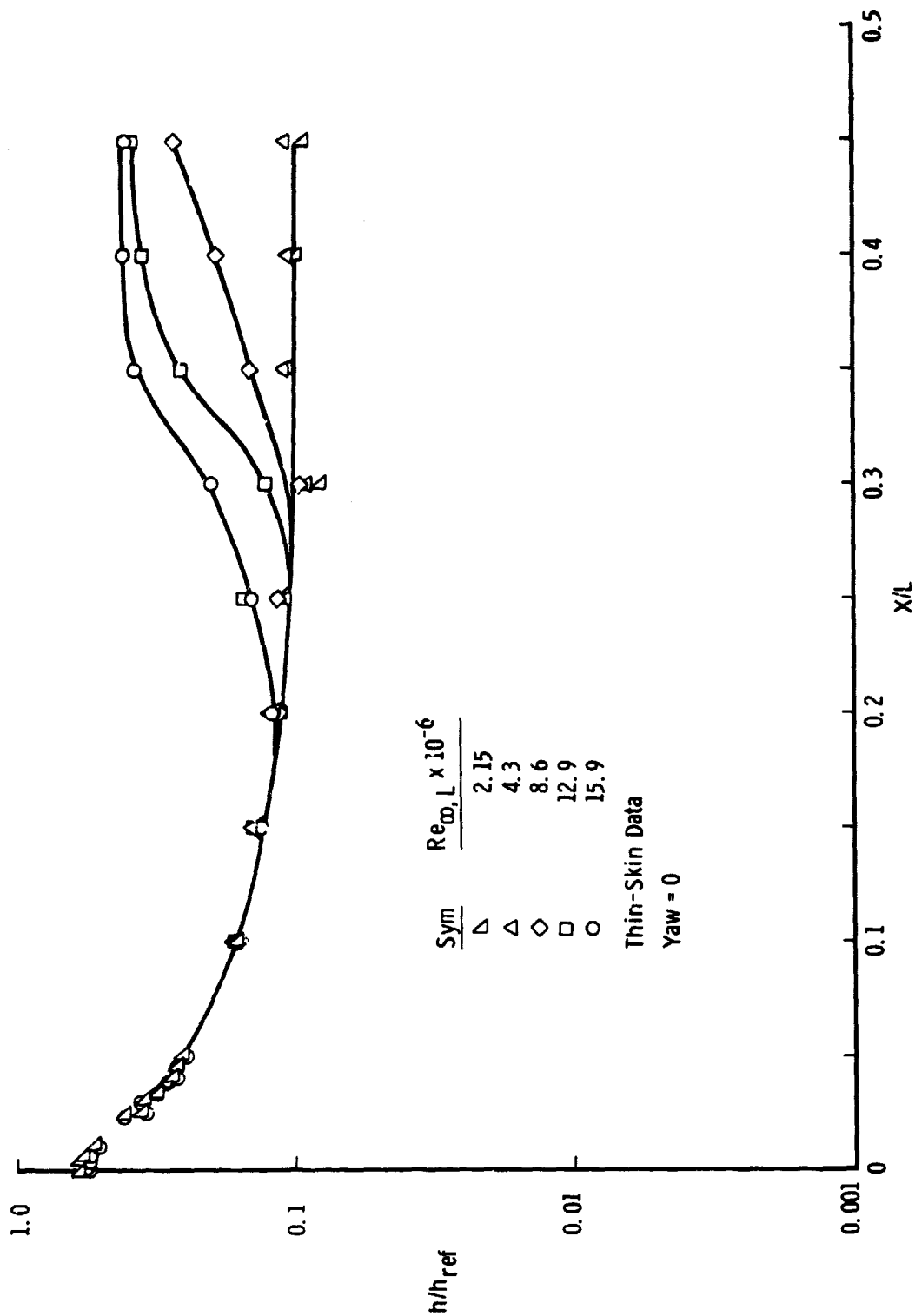
Figure 6. Windward centerline heat-transfer distributions at 40 deg angle of attack.
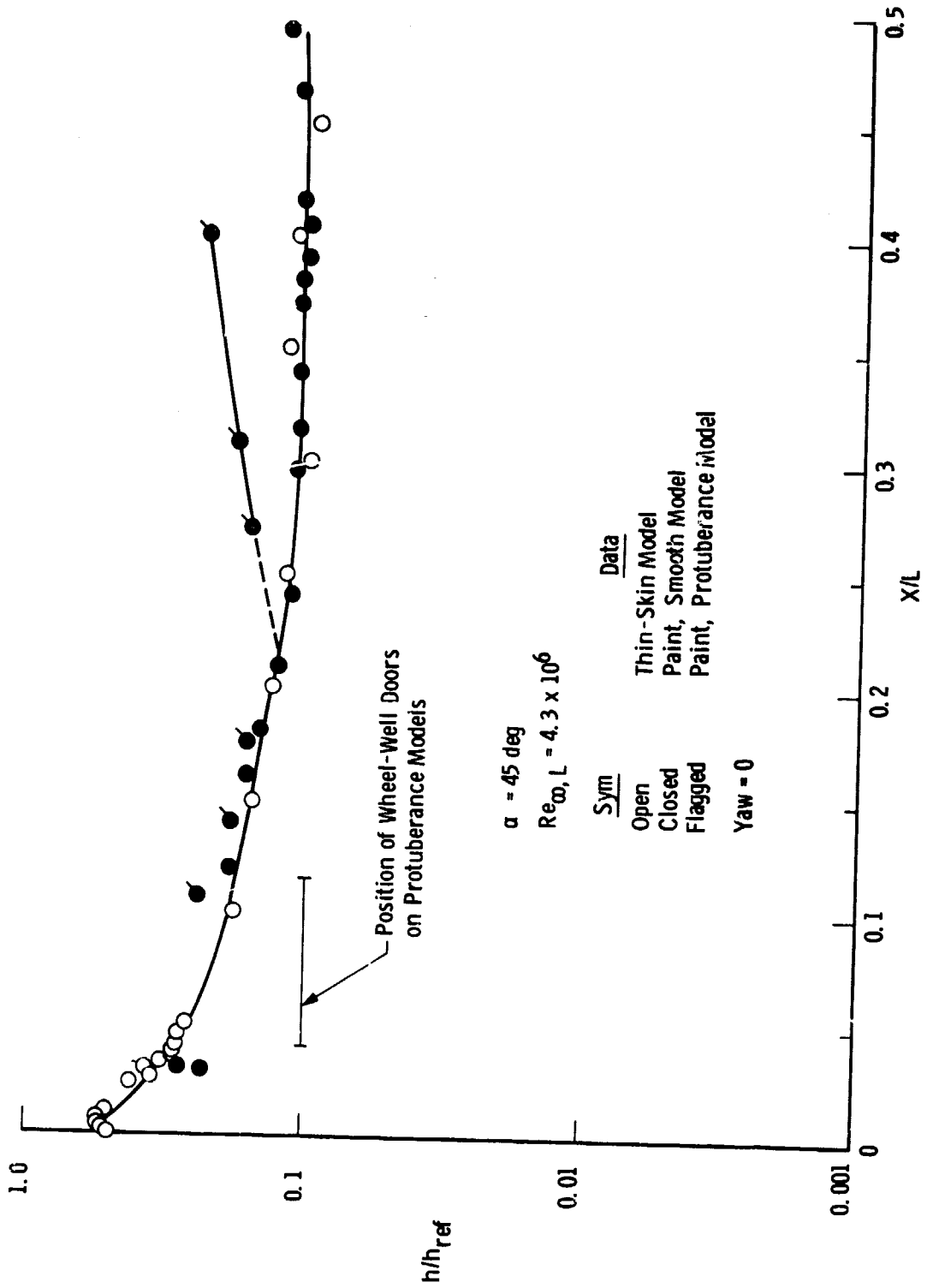
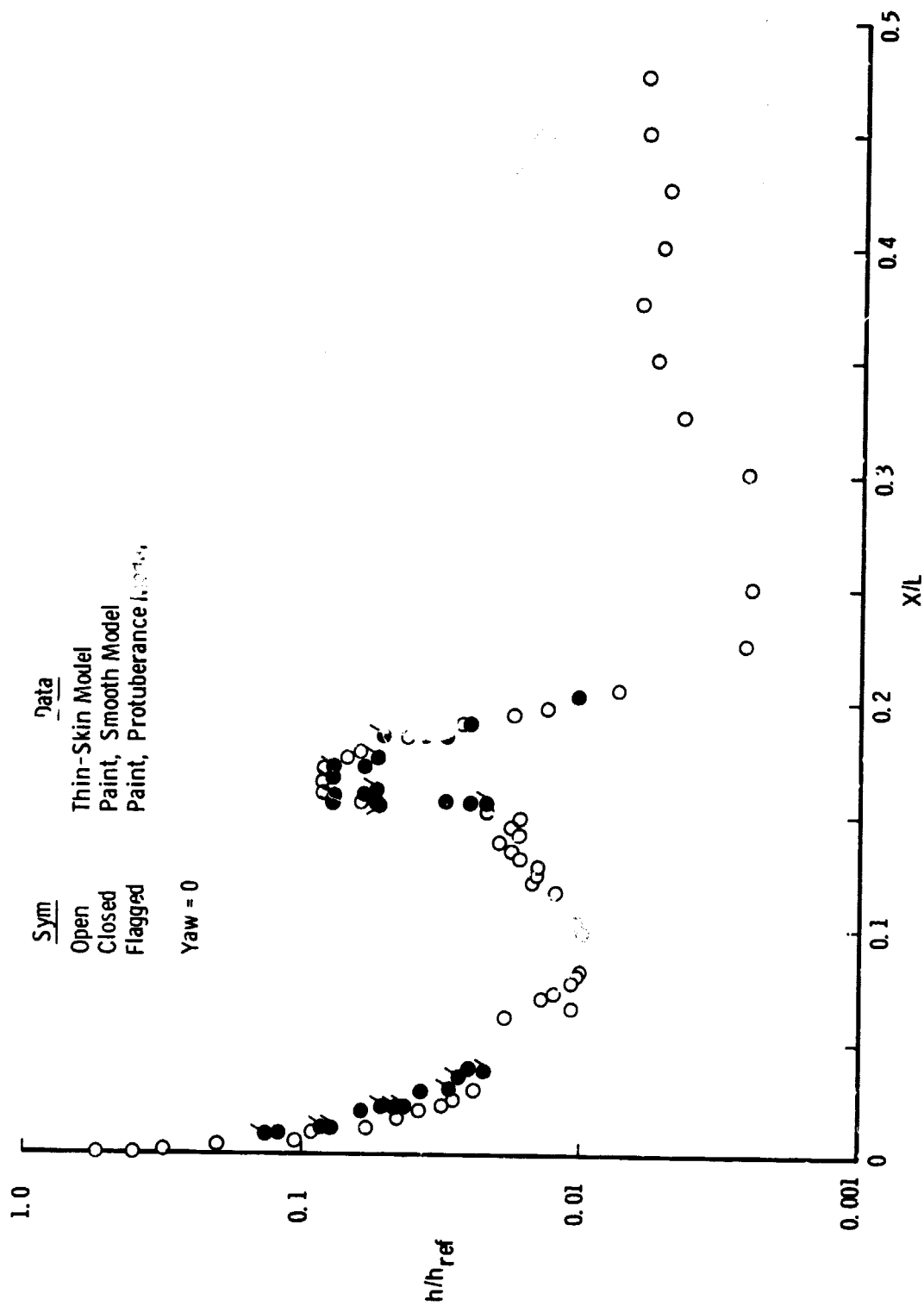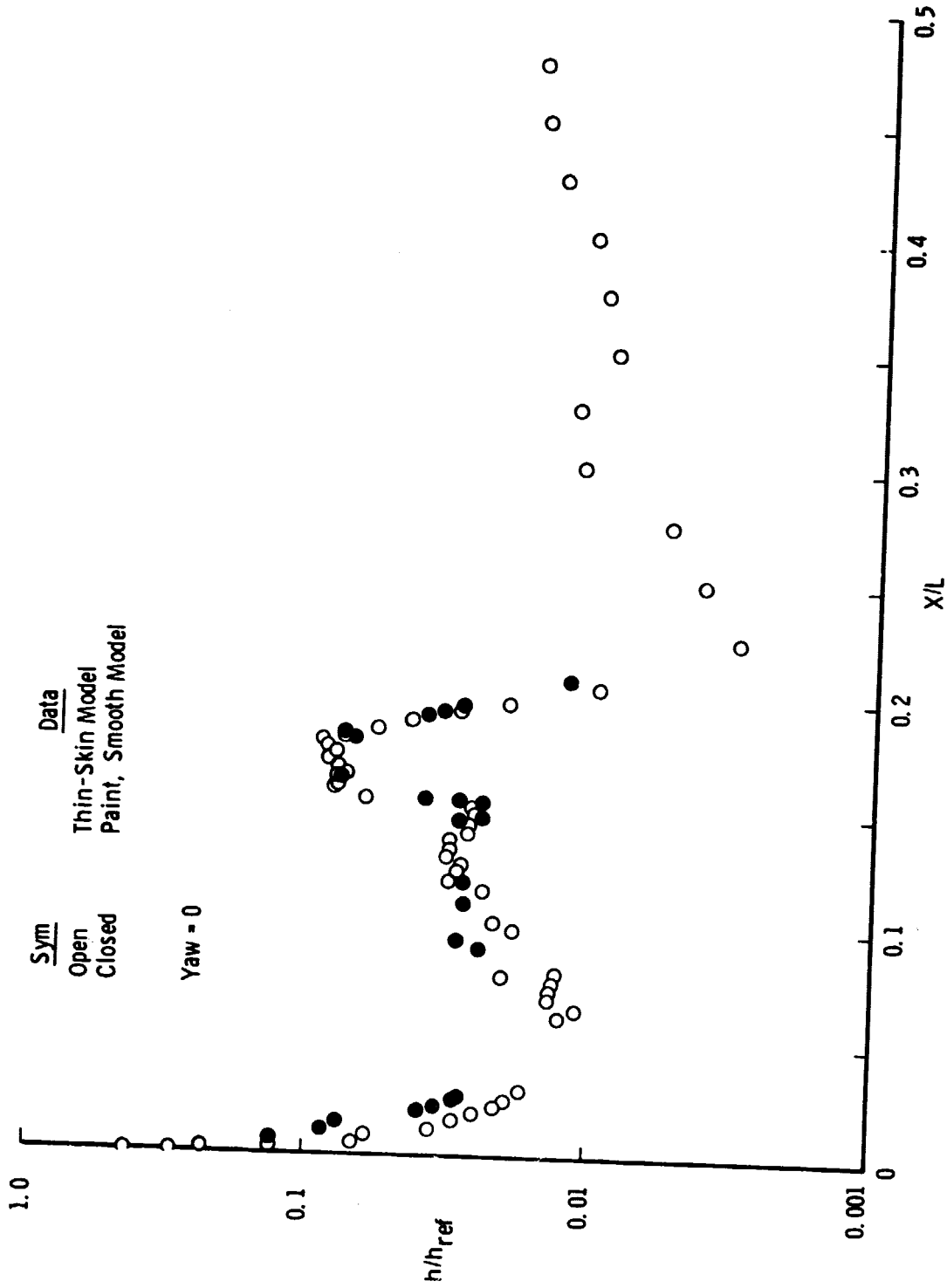Figure 7. Comparison of smooth and protuberance model windward centerline heat-transfer distributions.

a. $\alpha = 30$ deg

Figure 8. Leeward centerline heat-transfer distributions at $Re_{\infty, L} = 8.6 \times 10^6$.
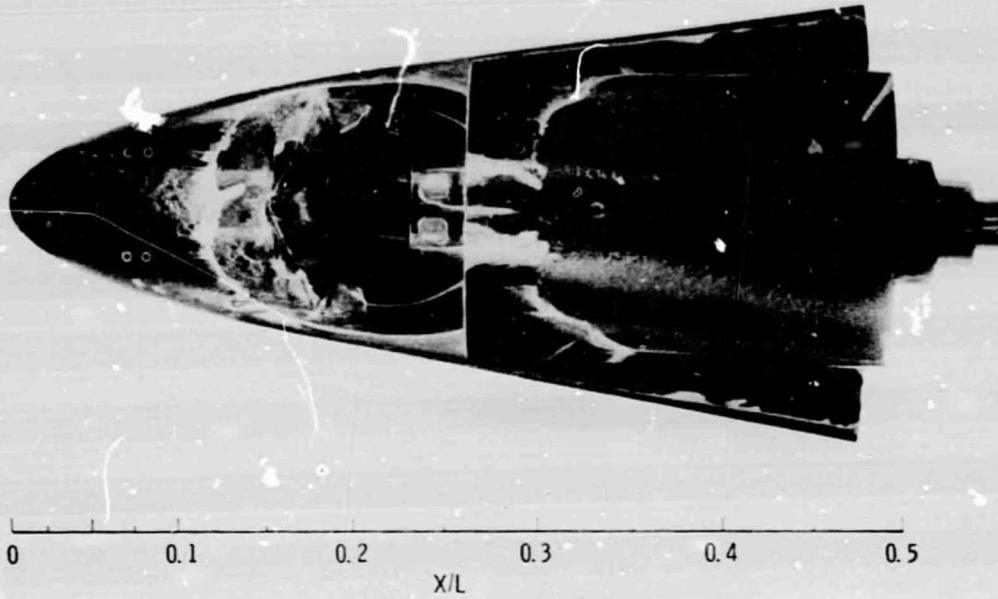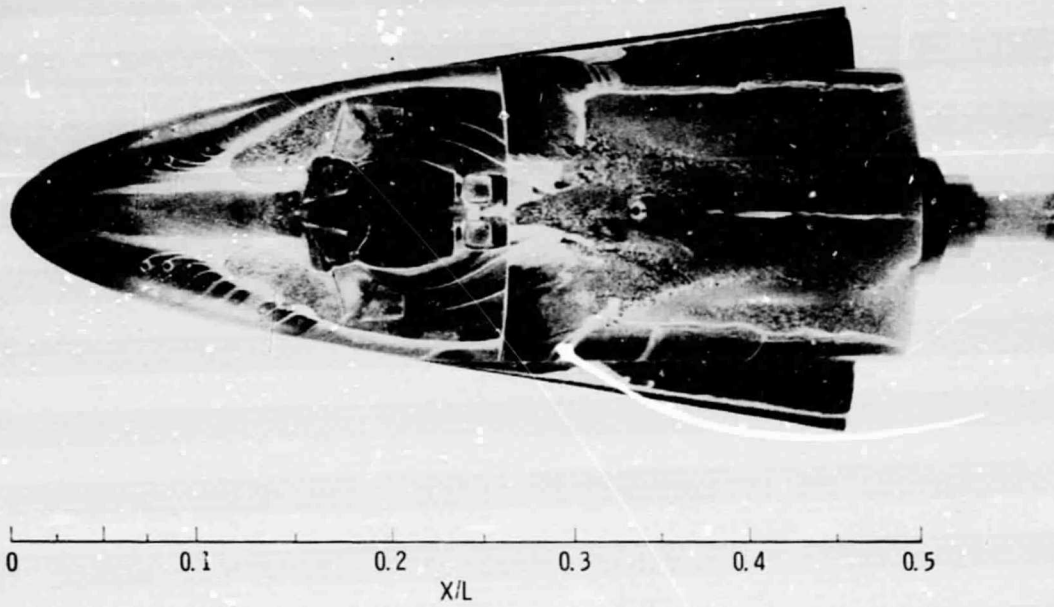
23

b. α = 40 deg
Figure 8. Concluded.
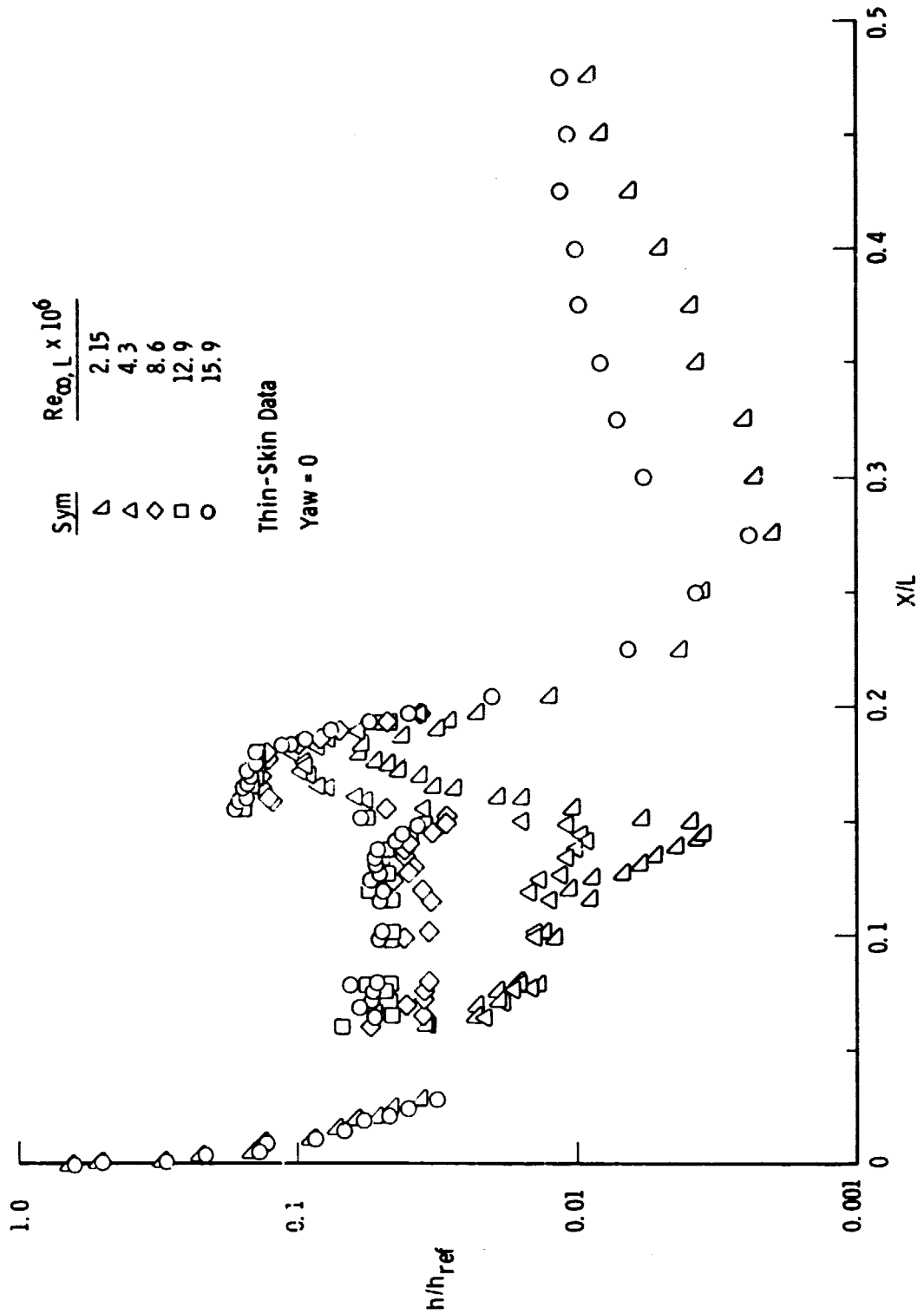
Figure 9.   Effects of Reynolds number on leeward centerline heat-transfer distributions at $a = 20$ deg.

0   0.1   0.2   0.3   0.4   0.5
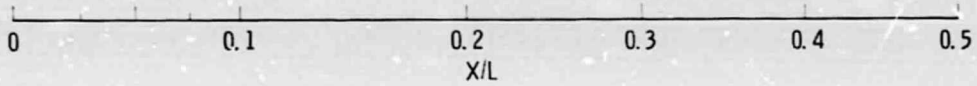   X/L

a. a = 20 deg (protuberance model)

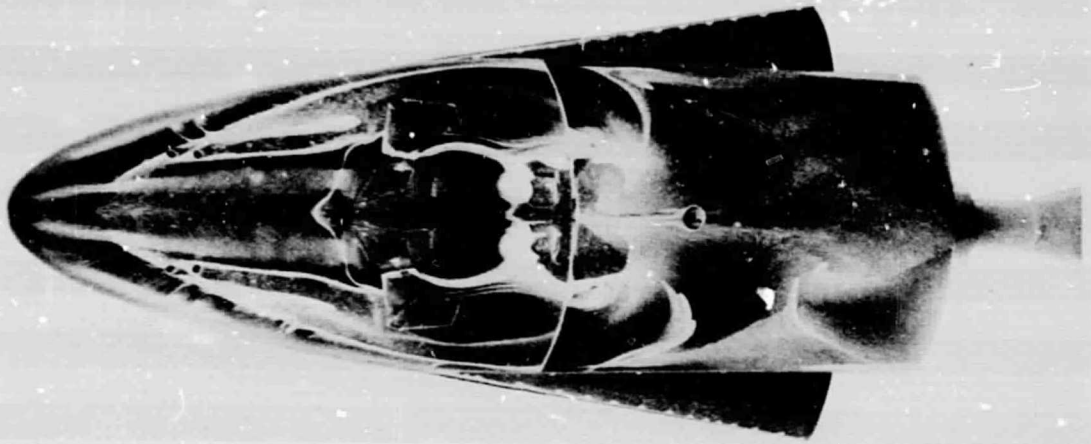0   0.1   0.2   0.3   0.4   0.5
                              X/L
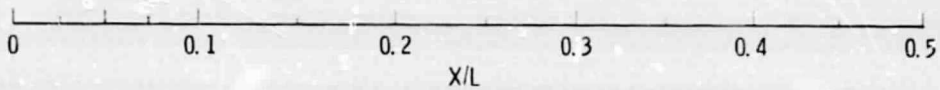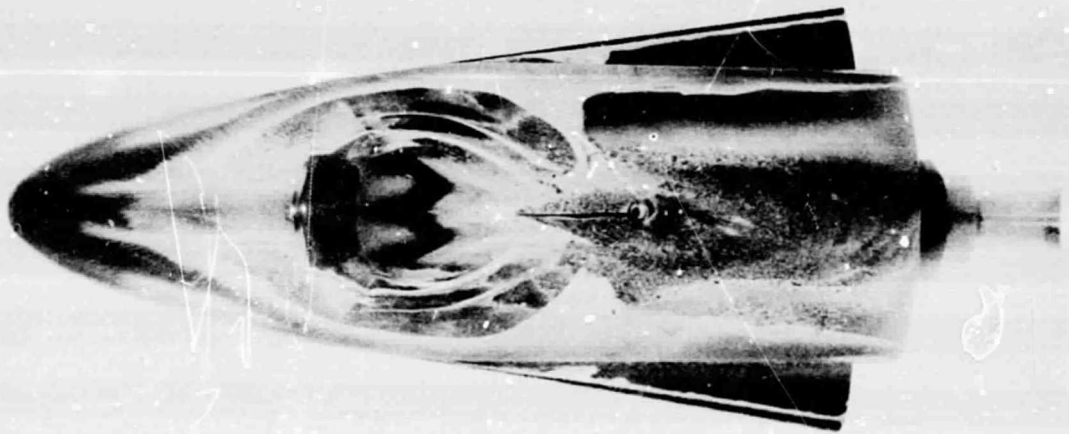
b. a = 30 deg (protuberance model)
Figure 10.   Leeward surface oil-flow photographs at $Re_{\infty, L}$ = 4.3 x 10^6.

c. a = 45 deg (protuberance model)

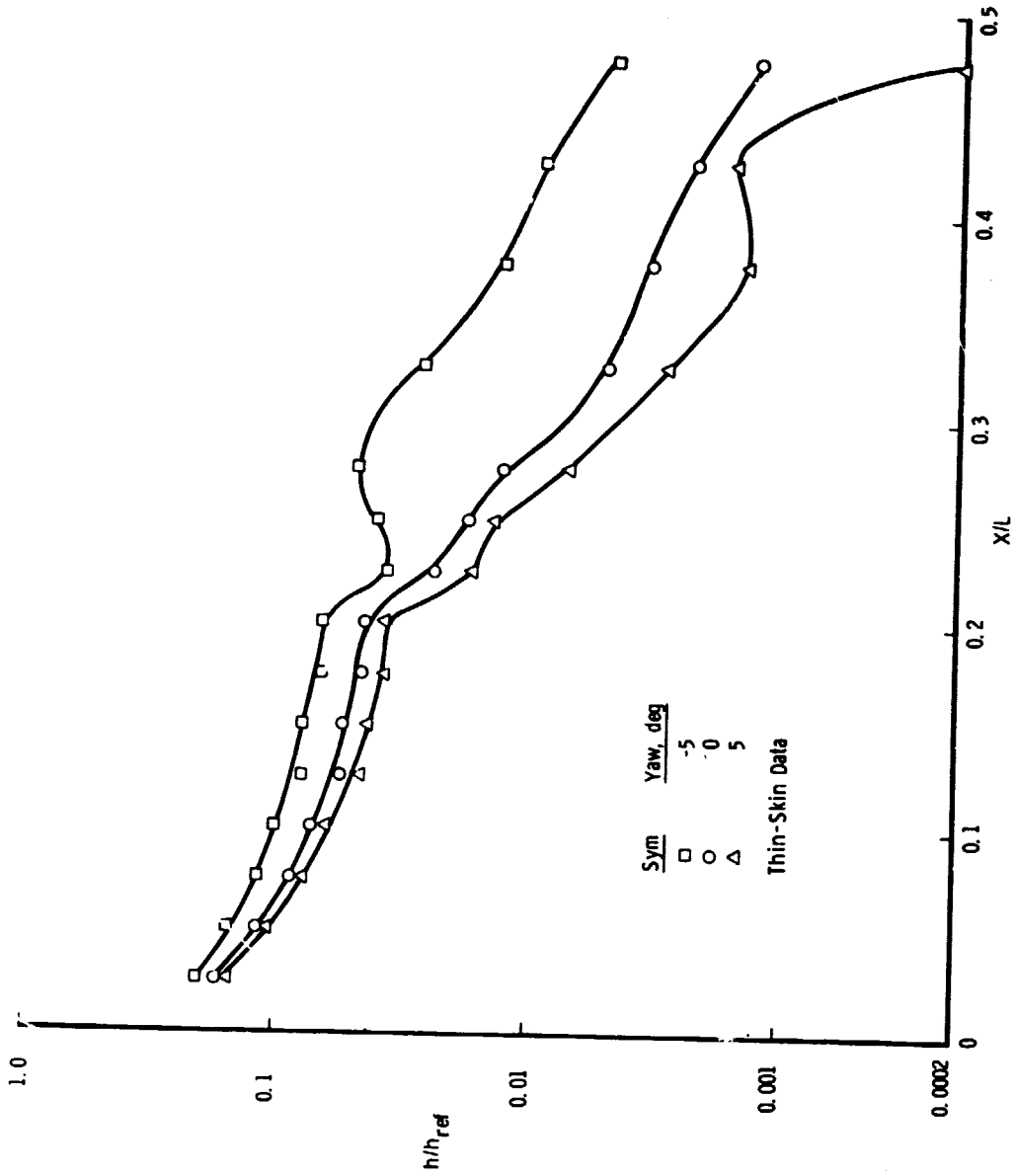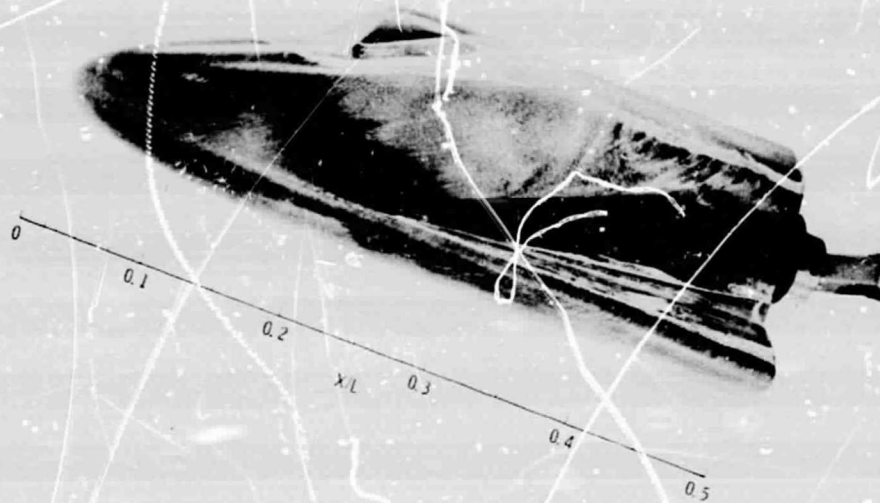d. a = 30 deg (smooth model)
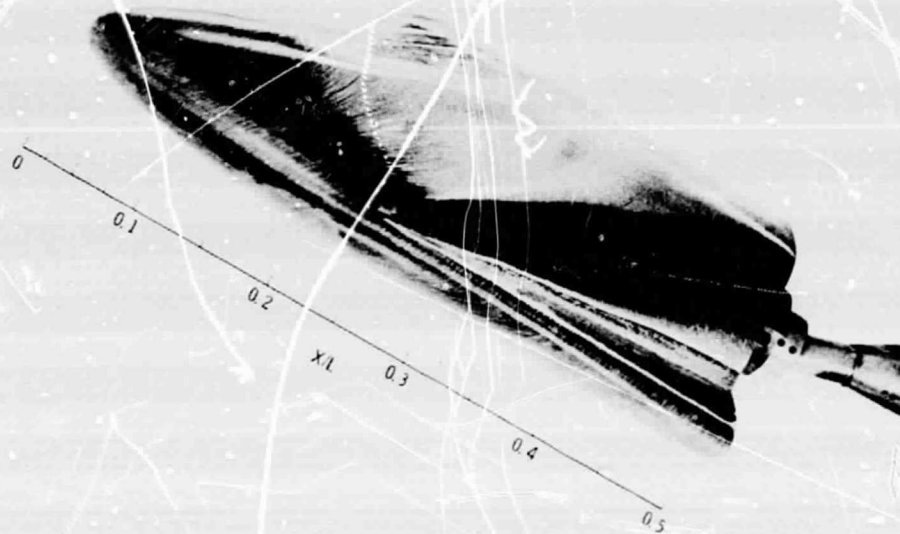Figure 10. Concluded.

Figure 11. Pilot-right-side maximum-half-breadth line heat-transfer distributions at $Re_{\infty,L} = 4.3 \times 10^6$, $\alpha = 20$ deg.
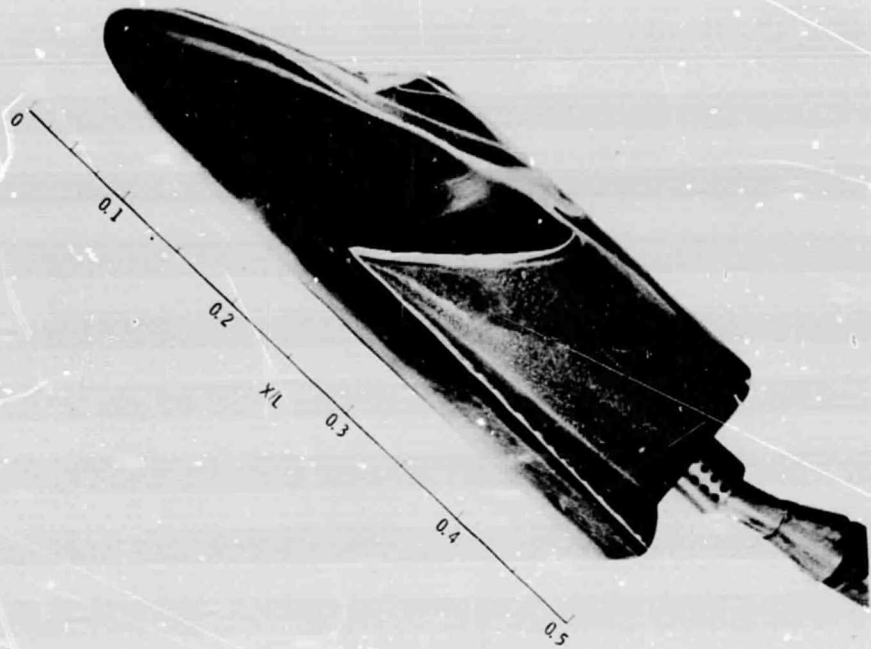
a. a = 20 deg (smooth model)
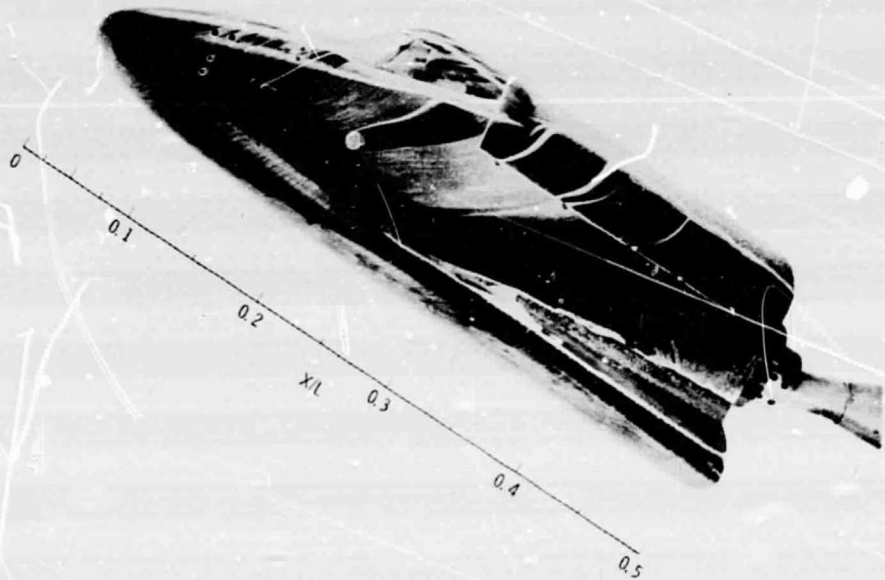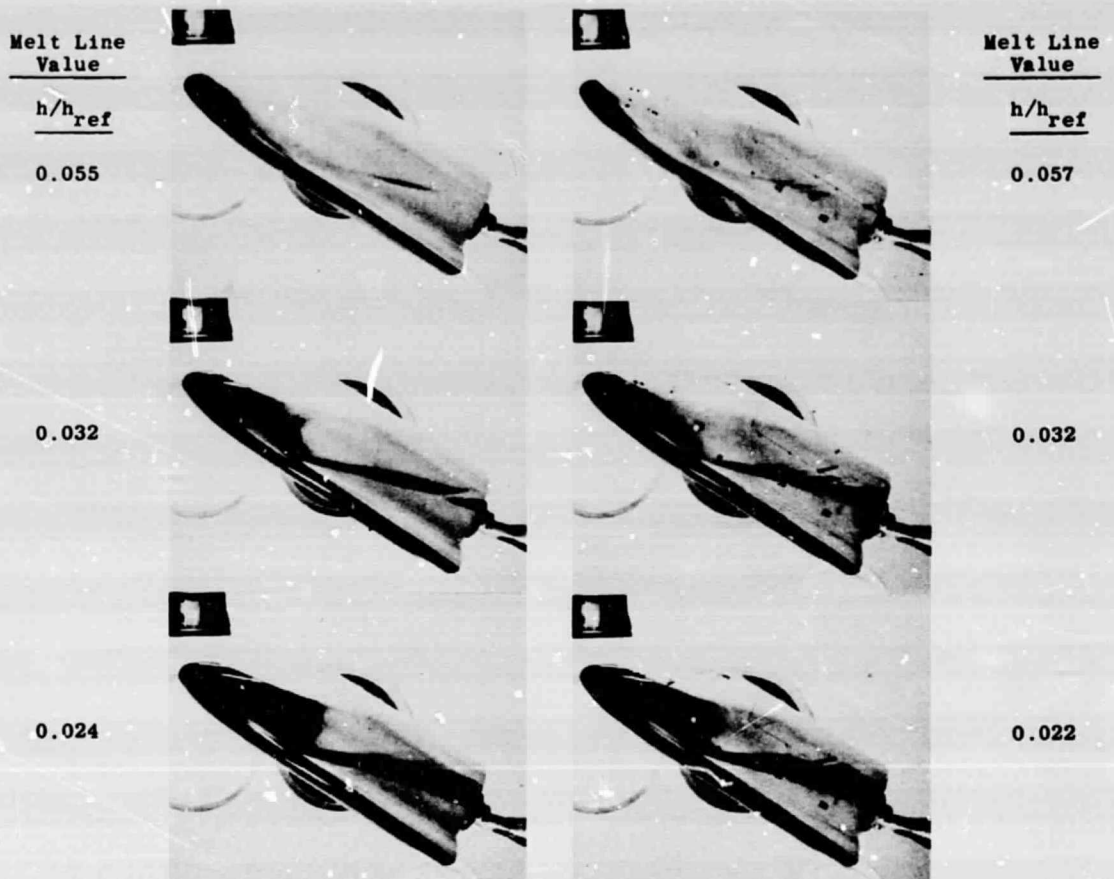

b. a = 30 deg (smooth model)

Figure 12. Pilot-left-side oil-flow photographs at $Re_{\infty,L}$ = 4.3 x 10^6.

c. a = 45 deg (smooth model)

d. a = 30 deg (protuberance model)
Figure 12. Concluded.

a. Smooth model   b. Protuberance model

Figure 13. Pilot-left-side phase-change paint photographs at
$Re_{\infty,L} = 4.3 \times 10^6$, $a = 30$ deg.

Table 1. Summary of Phase-Change Paint Tests

α, deg	$Re_\infty \times 10^{-6}$, ft^{-1}	M_∞	p_O, psia	T_O, °R	Yaw, deg
20	0.5	7.90	110	1,270	0
25					-1, 0, 1
30	↓	↓	↓		-1, 0, 1
20	1.0	7.94	210		0*
25					-1, 0, 1
30					-1, 0*, 1, 2
35					-1, 0, 1
40					0
45	↓	↓	↓	↓	0*
30	1.5	7.97	325	1,280	0
20	2.0	7.98	430	1,300	0
25					0
30					0
35					0
40					0
45	↓	↓	↓	↓	0

*Oil Flow

Table 2. Summary of Thin-Skin Thermocouple Tests

α, deg	$Re_\infty \times 10^{-6}$, ft^{-1}	M_∞	p_O, psia	T_O, °R	Yaw, deg
20	0.5	7.90	110	1,270	-2, 0, 2, 5
25					0
30					-2, 0, 2
35					0
40	↓	↓	↓	↓	0
20	1.0	7.94	210		-5, -2, 0, 2, 5
25					0
30					-2, 0, 2, 5
35					0
40					-2, 0, 2
45	↓	↓	↓	↓	0
20	2.0	7.98	430	1,300	-2, 0, 2
25					0
30					-2, 0, 2
35					0
40					-2, 0, 2
45	↓	↓	↓	↓	0
20	3.0	7.99	675	1,340	-5, -2, 0, 2, 5
25					0
30					-2, 0, 2, 5
35					0
40					-2, 0, 2
45	↓	↓	↓	↓	0
20	3.7	8.0C	860	1,350	-5, -2, 0, 2, 5
25					0
30					-2, 0, 2, 5
35					0
40	↓	↓	↓	↓	-2, 0, 2

Table 3. Material LH Thermophysical Properties

T_{pc}, °F	k, Btu/ft-hr-°R	c_p, Btu/lbm-°R	w, lbm/ft³	$\dfrac{\sqrt{wc_pk}}{\text{Btu/ft}^2\text{-°R-(sec}^{1/2})}$
113	0.272	0.249	125.4	0.0486
125	0.271	0.257	125.4	0.0493
131	0.271	0.262	125.4	0.0497
150	0.270	0.271	125.4	0.0505
169	0.270	0.282	125.4	0.0515
175	0.270	0.285	125.4	0.0518
200	0.269	0.299	125.4	0.0529
225	0.268	0.313	125.4	0.0541
250	0.267	0.326	125.4	0.0551
275	0.266	0.338	125.4	0.0560
300	0.265	0.350	125.4	0.0568
325	0.264	0.358	125.4	0.0574
350	0.262	0.367	125.4	0.0579
400	0.260	0.378	125.4	0.0585

NOMENCLATURE

b	Model skin thickness, ft
c_p	Specific heat, Btu/lbm-°R
h	Heat-transfer coefficient, $\dot{q}/(T_o - T_w)$, Btu/ft²-sec-°R
k	Model material conductivity, Btu/ft-hr-°R
L	Scaled axial length of Orbiter, 51.6 in.
M	Mach number
p_o	Stilling chamber pressure, psia
$\dot{q}$	Heat transfer rate, Btu/ft²-sec
Re	Unit Reynolds number, ft⁻¹
$Re_{\infty,L}$	Free-stream Reynolds number based on L
T	Temperature, °F or °R as noted
t	Time, sec
Δt	Time increment that model has been exposed to uniform flow, sec
w	Model material density, lbm/ft³
X	Axial distance from model nose, in.
yaw	Yaw angle, deg
α	Angle of attack, deg
β	Semi-infinite heating equation parameter $(h\sqrt{\Delta t}/\sqrt{wc_p k})$

SUBSCRIPTS

aw	Adiabatic wall conditions
i	Initial conditions
o	Stilling chamber conditions

35

pc   Phase change

ref   Heat-transfer parameter based on Fay-Riddell theory and a 1-ft nose radius
            scaled down to the model scale (i.e., 0.04 ft)

w   Wall conditions

∞   Free-stream conditions